



Contents lists available at SCCE

Journal of Soft Computing in Civil Engineering

Journal homepage: www.jsoftcivil.com



Optimal Design of MR Dampers Using NSGA-II Algorithm

Mehdi Babaei^{1*} , Nastaran Taghaddosi², Navid Seraji²

1. Assistant Professor, Department of Civil Engineering, Faculty of Engineering, University of Zanjan, Zanjan, Iran

2. Department of Civil Engineering, Faculty of Engineering, University of Zanjan, Zanjan, Iran

Corresponding author: mbabaei@znu.ac.ir

 <https://doi.org/10.22115/SCCE.2022.347247.1466>

ARTICLE INFO

Article history:

Received: 14 June 2022

Revised: 04 December 2022

Accepted: 26 December 2022

Keywords:

Semi-active control;

MR damper;

Multi-objective optimization;

Fuzzy logic;

NSGA-II algorithm.

ABSTRACT

In recent years, new ideas and solutions have been proposed by scientists and researchers to control the response of structures against seismic excitations. In this article, The Optimization of semi-active control systems using MR dampers has been studied to reduce the structure's response under earthquake forces. For this purpose, three frames of five, eight, and eleven stories have been examined as numerical examples. A multi-objective optimization approach based on the NSGA-II algorithm is used to control the response of structures and the fuzzy logic algorithm is used to determine the force of these dampers. The values of maximum displacement, acceleration, and inter-story drift of the top floor have been selected as objective functions. The position of dampers has been optimized to obtain optimal practical solutions. The results show that the responses are significantly reduced when using a semi-active MR damper and the arrangement of the dampers has a great impact on the amount of this reduction.

1. Introduction

Controlling the response of structures against seismic excitations has always been one of the challenges of the structural engineering field. In recent years, new ideas and solutions have been

How to cite this article: Babaei M, Taghaddosi N, Seraji N. Optimal design of MR dampers using NSGA-II algorithm. J Soft Comput Civ Eng 2023;7(1):72-92. <https://doi.org/10.22115/scce.2022.347247.1466>

2588-2872/ © 2022 The Authors. Published by Pouyan Press.

This is an open access article under the CC BY license (<http://creativecommons.org/licenses/by/4.0/>).



proposed by scientists and researchers to reduce the structural response due to the effects of dynamic forces, the most important of which is the use of structural control systems. Tuned mass [1] and magneto-rheological dampers [2] are the most famous instruments to control and absorb earthquake loads. One important type of these systems is the semi-active control system.

In the semi-active control system, the required external energy is much smaller in size than in conventional active control systems, also while maintaining the reliability of passive control systems, it has advantages such as adjustable parametric characteristics of the active control system [3]. In these systems, the control action is achieved by the movement of the structure and regulated by an external energy source, and while determining the response of the structure at any time using a force control algorithm, the required amount of force can be changed.

Magnetorheological fluid dampers are modern control devices for structures having features such as small size, low energy consumption, adjustable force, high force capacity, fast response, and safe operation in the event of damage. These dampers are usually composed of a hydraulic cylinder containing micron-sized, magnetically polarized particles suspended inside an oily fluid [4]. In MR dampers, the viscosity of the fluid inside them can be changed. This change in viscosity occurs with an increase or decrease in the intensity of the magnetic field and changes the hardness and yield stress of these dampers. As a result, their energy absorption can change at any time. The damping force in an MR damper is a nonlinear function of voltage and velocity at both ends. The fluctuation in the damping ratio is obtained by changing the input voltage to the damper [5].

An important issue in the seismic control of structures is the position and number of control systems that must be determined and optimized for economic purposes [6–8]. Dyke and Spencer used the MR damper in 1996 to control a three-story structure [9]. The three-story model structure was subjected to the El Centro earthquake, and the MR dampers were set on two consecutive lower floors. The results showed that the acceleration and displacement of the structure decreased in the semi-active control. In 2001, Qu et al. Conducted a study on the use of ER/MR dampers to control the seismic responses of a structure containing a tower and a podium structure [10].

The ER/MR dampers were used to reduce the whipping effect on the tower structure and reduce the seismic responses of both the tower structure and the podium structure. In 2003, Zhou et al. used an adaptive fuzzy control strategy for protecting buildings against dynamic hazards, such as severe earthquakes and strong winds. The researchers concluded that the use of MR dampers reduced the response of linear and nonlinear multiple degrees of freedom systems [11]. In 2004, Renzi and Serino tested a four-story steel frame equipped with a bracing system including magnetorheological (MR) dampers operating in both passive and semi-active on a shaking table [12]. The structure was affected by two natural accelerograms. The results showed that under semi-active control, the structure's displacement was reduced by about 30 to 35% more than the passive one.

In 2006, Yan and Zhou controlled vibrations using a fuzzy controller and MR damper in a three-story structure [13]. In this study, a genetic optimization algorithm was used to control the

vibrations of structures under the El Centro earthquake. The researchers concluded that in the case of using the semi-active control with the fuzzy optimized algorithm, displacement responses, and accelerations are effectively reduced. In 2012, Amini and Ghaderi used the improved ant colony algorithm to find the optimal location of three and four MR dampers in an eight-story and ten-story linear structure using only one shear force as the objective function [14]. In 2017, Askari et al. applied the genetic algorithm multi-objective optimization method to find the optimal location of a certain number of semi-active and active MR dampers in a twenty-story nonlinear structure [15]. They used LQG and clipped-optimal algorithms to regulate the input voltage of the MR damper. The results show that the MR dampers in optimal locations perform better in reducing inter-story drift. Instead, active dampers in the optimal positions work better at reducing the maximum acceleration and base shear.

2. NSGA-II algorithm

For solving optimization problems, there are a myriad of meta-heuristic algorithms and each one has its unique method of finding the optimum solution (e.g., ACO, ABC, PSO, GA, SBO, etc.) [16–30]. Also, there are plenty of studies related to the performance of these meta-heuristics on multi-objective optimizations [31–33].

In this study, the well-known evolutionary algorithm NSGA-II was used since it has shown its capabilities for solving various multi-objective optimization problems in recent years. It was first proposed by Deb and his colleagues in 2000 based on the genetic algorithm (GA) to enhance its capabilities in multi-objective optimization. Unlike the single objective optimization technique, non-dominated sorting algorithm II (NSGA-II) simultaneously optimizes each objective without being dominated by any other solution. Fig 1. demonstrates how the NSGA-II algorithm works. This algorithm has been applied for multi-objective optimization of steel buildings considering probabilistic performance-based design parameters [34,35].

3. Model of MR dampers

To develop control algorithms that take full advantage of the MR dampers, models must be defined that can accurately describe the inherent nonlinear behavior of dampers. To model the behavior of the MR damper, the Bouc-Wen behavioral model was used. In structural engineering, the Bouc–Wen model of hysteresis is one of the most used hysteretic models typically employed to describe non-linear hysteretic systems. It was introduced by Robert Bouc and extended by Yi-Kwei Wen, who demonstrated its versatility by producing a variety of hysteretic patterns. This model is able to capture, in analytical form, a range of hysteretic cycle shapes matching the behavior of a wide class of hysteretic systems. Due to its versatility and mathematical tractability, the Bouc–Wen model has gained popularity. Instead of modeling the MR damper itself, the force generated by it enters the model. The Bouc-Wen behavioral model for MR dampers consists of a Bouc-Wen element and a linear damper, which operate in parallel [36]. An overview of this behavioral model is shown in Figure 2.

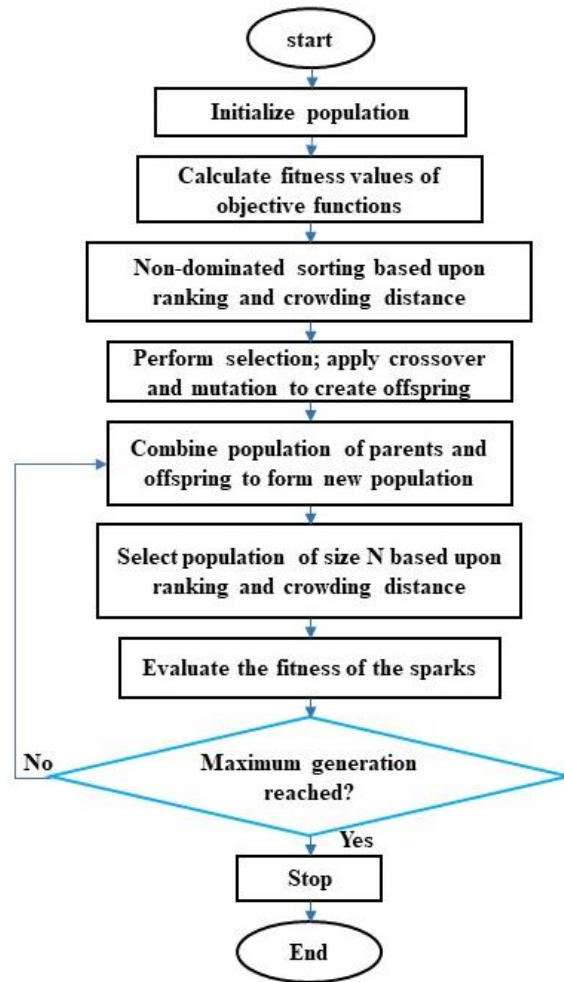


Fig. 1. Flowchart of the NSGA-II algorithm.

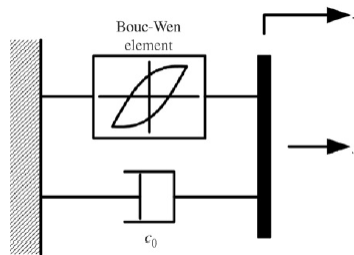


Fig. 2. Bouc-Wen Behavioral Model for MR Dampers [37].

The force generated by the damper in this model is calculated through Equation (1):

$$F = C_0 \dot{x} + \alpha z \tag{1}$$

$$\dot{z} = -\gamma |\dot{x}| z |z|^{n-1} - \beta \dot{x} |z|^n + A_m \dot{x} \tag{2}$$

In Equations (1) and (2), F is the damping force, x is the damping displacement, z is the evolutionary variable, and the parameters n , γ , β , and A_m are fixed values that are determined experimentally on each damper. The parameters C_0 and α are determined using Equations (3) and (4):

$$\alpha = \alpha(u) = \alpha_a + \alpha_b u \quad (3)$$

$$C_0 = C_0(u) = C_{0a} + C_{0b} u \quad (4)$$

In these equations, the applied control voltage u and the parameters α_a , α_b , C_{0a} , C_{0b} are constant values. With nine fixed damper parameters, a Bouc-Wen behavioral model can be created.

In this study, an MR damper with a capacity of 1000 KN was used. The input voltage of the dampers can vary between zero and 10 volts. The optimal maximum voltage value for this model is 3.5 volts. The parameters for simulating the behavior of MR dampers are shown in Table 1.

Table 1

Parameters for simulating the behavior of MR dampers.

Parameter	Value	Parameter	Value	Parameter	Value
β	3.0 (cm ⁻¹)	C_{0b}	44.0 × 10 ⁵ (Ns/cm/V)	α_a	1.0872 × 10 ⁵ (N/cm)
γ	3.0 (cm ⁻¹)	A_m	1.2	α_b	4.9616 × 10 ⁵ (Ns/cm)
η	50 (s ⁻¹)	n	1	C_{0a}	4.40 (Ns/cm)

One of the limitations of MR dampers is the time delay in applying the control force. The value of this delay, depending on the type of damper is about 0.02 to 0.1 seconds.

Equation (5) is used to model this slight delay in the system.

$$u = -\eta(u - v) \quad (5)$$

In this equation v is the command voltage and η is a constant value. To model the behavior of the MR damper, its behavioral equations are solved as recursive equations.

4. Optimization process

In this study, the positions of dampers are considered as design variables, which is a vector containing zero and one values. The vector is sent as an input to the Simulink model. All AISC design code requirements are considered constraints including stresses and displacements. After applying the earthquake force, the response of the damper is applied to the structure in each step of the earthquake. Consequently, the objective functions, which include either the maximum displacement and acceleration or the maximum inter-story displacement and acceleration, are sent to the algorithm as output. Thenceforth, the responses are sorted and queued after

determining the crowding distance. Then, the first front of the answers is determined by using the crossover and mutation operators. In this study, the crossover rate is 0.7 and the mutation rate is 0.3.

Figure 3 shows the Simulink model of motion equation of the structure with the MR damper.

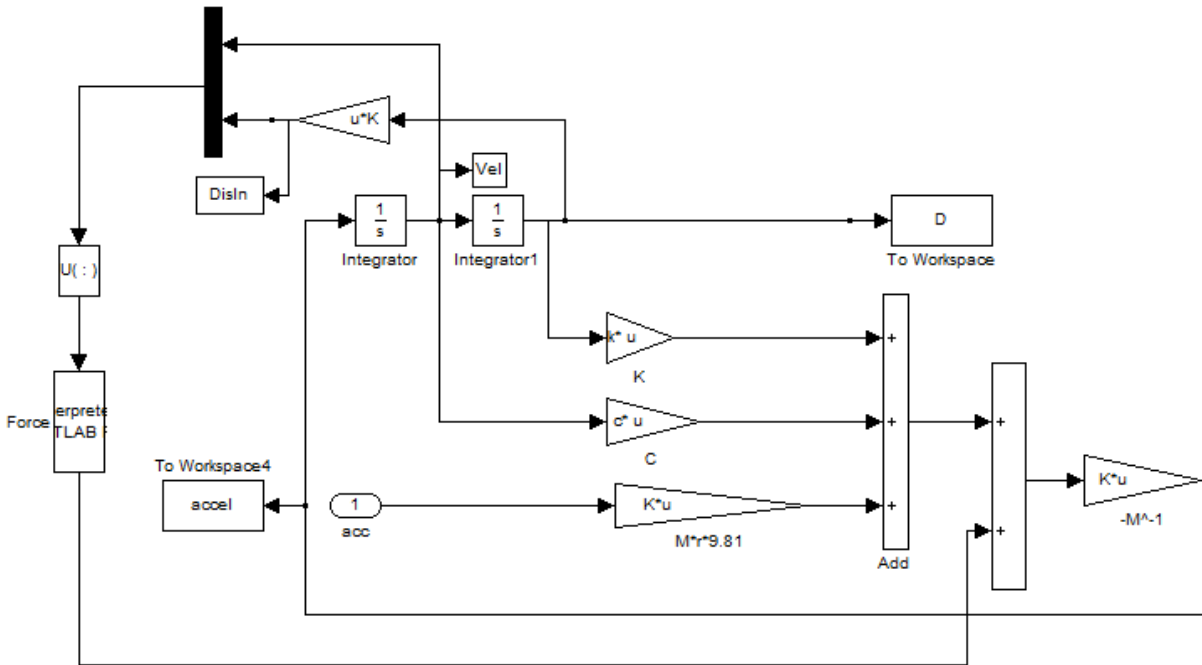


Fig. 3. Simulink model of structure's motion equation with MR damper.

To investigate the structural response, the equations of motion of the structure in both controlled and uncontrolled states are created in Simulink. In the semi-active mode, a Mamdani fuzzy controller is used with two inputs and one output. The inputs are displacements and the relative speed of the floors, while the output is the damper voltage. To control the response of the structure, a two-objective optimization is used based on the NSGA-II algorithm. The NSGA-II algorithm is one of the best metaheuristics for solving multi-objective functions. The maximum displacement and acceleration of the highest floor of the structure are selected as the objective functions in the first problem and the maximum inter-story drift and acceleration of the highest floor are selected as the objective functions in the second problem. To satisfy these functions, the positions of MR dampers in the structure were optimized.

5. Experimental setup

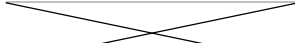


5.1. Details of the frames

To evaluate and compare the performance of the control system, numerical studies have been performed on five, eight, and eleven-story steel frames. All of the structures are hypothetical schools located in Tehran. The design base acceleration is considered as 0.35, and the importance

factor for important structures such as schools is considered as 1.2. Chevron braces are used in the middle span of the structures. The natural frequency of a five-story, eight-story and eleven-story structure is respectively 0.37 seconds, 0.68 seconds, and 0.92 seconds.

The frame specifications are presented in Table 2 and figures 4, 5, and 6.

Table 2
Specifications of five, eight, and eleven-story frames.

Type	Sections		
	Five-story	Eight-story	Eleven-story
1	W14x48	W16x50	W16x67
2	W16x57	W14x30	W14x159
3	W14x30	W14x22	W14x120
4	W14x22	W14x48	W14x48
5	W14x26	W16x89	W14x30
6		W16x67	W14x22
7		W14x26	W18x35
8			W16x26

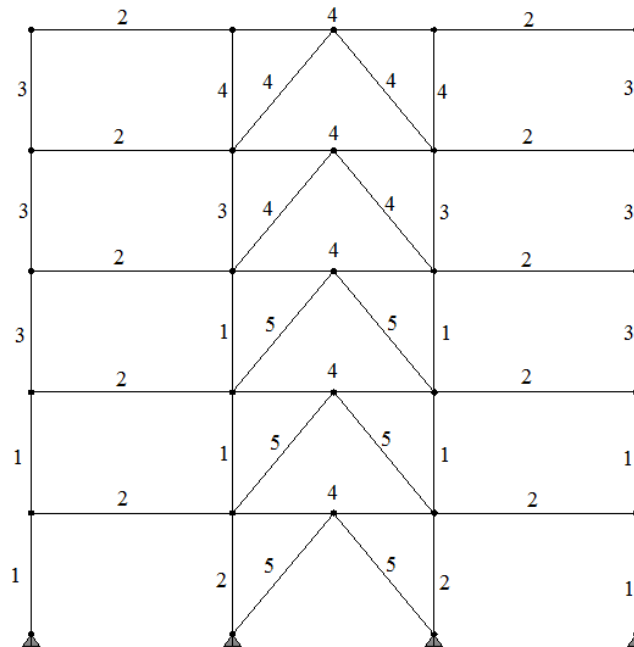


Fig. 4. Five-story structure with Chevron bracing.

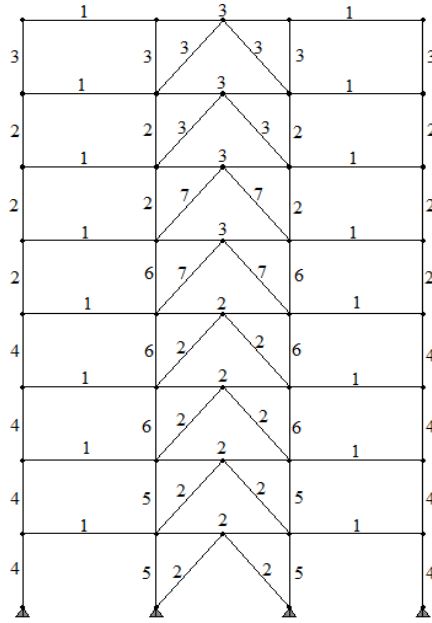


Fig. 5. Eight-story structure with Chevron bracing.

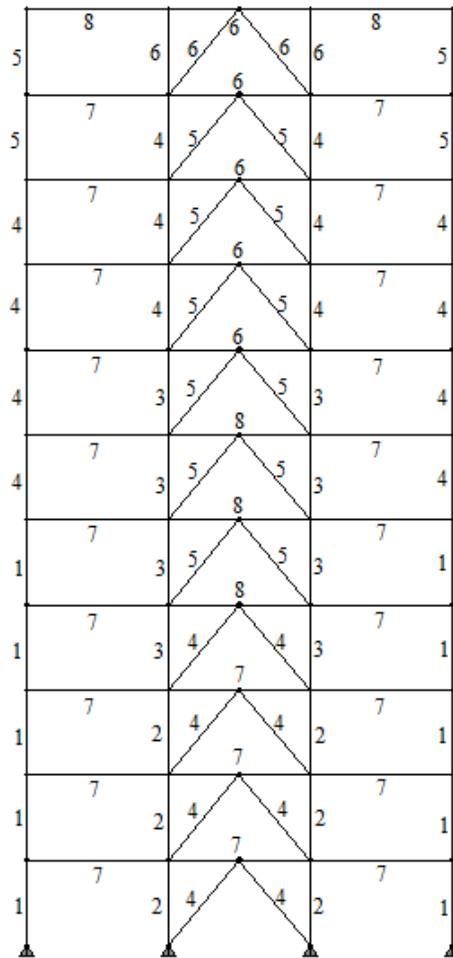


Fig. 6. Eleven-story structure with Chevron bracing.

5.2 Horizontal accelerogram of the earthquakes used

The analyses performed in this study are of linear time history analysis, and the earthquake records are applied horizontally to the structures. To perform time history analysis, seven far-field earthquake records are used, which are mentioned in Table 3. The Peak Ground Acceleration (PGA) is expressed in fractions of g ($1 g = 9.81 \text{ m/s}^2$).

Table 3
Selected Earthquake Records.

Earthquake	Station	Magnitude (ML)	PGA
Imperial Valley 1979	Cerro Prieto	6.5	0.21
Kobse 1995	Nishi-Akashi	6.9	0.509
Kocaeli Turkey 1999	Arcelik	7.6	0.21
Landers 1992	Superstition Hills	7.3	0.446
Loma Prieta 1989	Capitola	6.9	0.528
Manjil Iran 1990	Abbar	7.4	0.514
Southern Calif 1989	San Luis Obispo	6.9	0.049

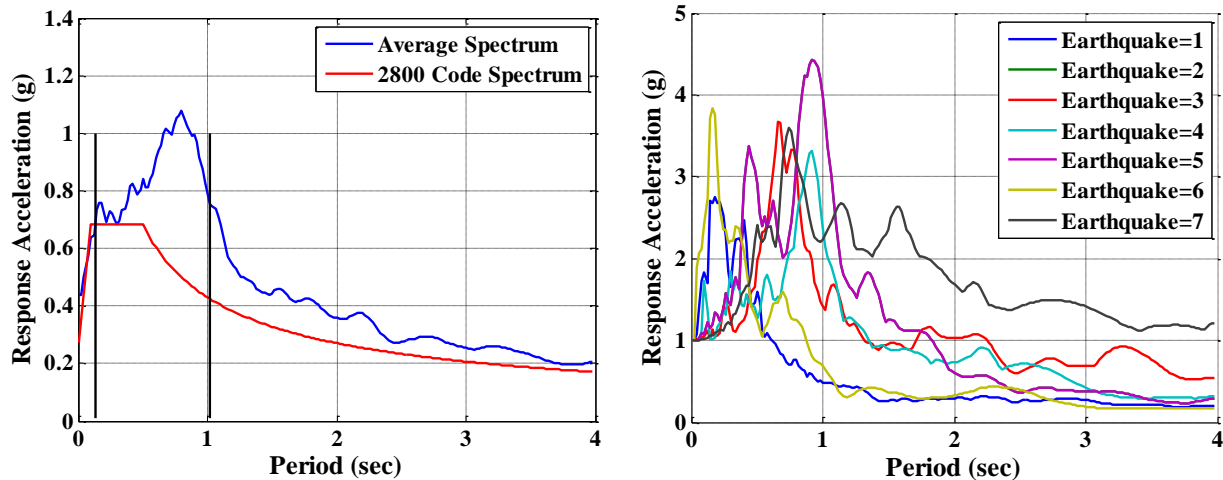


Fig. 7. The response spectrum of earthquakes applied to the structure

Figure 7. shows the response spectrum of earthquakes applied to the structure (left figure) and compares the average spectrum and the code's design spectrum of the five-story frame (right figure).

The values of the earthquake scale factor of all three frames are given in Table 4.

Table 4
Frames scale factor.

Number of Stories	Scale Factor
5	0.4686
8	0.432
11	0.432

5.3. Behavior validation of MR dampers

To ensure that the behavior of the MR damper in the structural model is flawless, the damper is subjected to a cyclic deformation, and a diagram of the force generated by it for zero, five, and 10 volts is drawn. Figure 8 demonstrates the force diagram of dampers obtained from the present study which is similar to the graph attained by Ok et al. in 2007. Comparing the diagrams for all three voltages in the present study, it can be seen that the behavior of the MR damper is modeled close to reality.

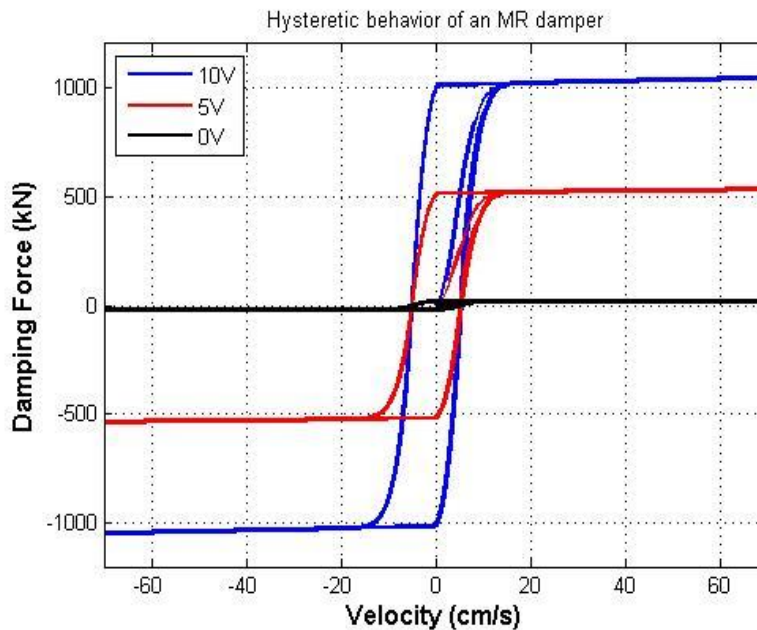


Fig. 8. MR damper behavioral diagram in this study.

6. Experimental results

6.1. Five-story structure

According to the results obtained from the five-story frame, the optimal position for the MR damper is on the fifth floor. The stories selected for the three-damper mode are first, third, and fifth. The results for both modes are shown in Tables 5 and 6.

Table 5

Five-story frame responses for placing the damper on the fifth floor.

Earthquake	Max. roof displacement (m)	Reduction (%)	Max. roof acceleration (m/s^2)	Reduction (%)	Max. roof drift (m)	Reduction (%)
Imperial Valley	0.0139	20	7.736	18.8	0.0028	12.5
Kobe	0.0361	32	13.1298	-2	0.0062	19
Kocaeli Turkey	0.0163	27.8	8.4072	26.6	0.0033	13
Landers	0.025	47.9	9.2465	27.8	0.0042	45
Loma Prieta	0.0472	46	21.8786	20	0.0085	44
Manjil Iran	0.0362	33	18.7536	0.7	0.0077	22
Southern Calif	0.0343	36	12.1474	30.8	0.0059	36.5

Table 6

Five-story frame responses for placing three dampers on floors one, three and five.

Earthquake	Max. roof displacement (m)	Reduction (%)	Max. roof acceleration (m/s^2)	Reduction (%)	Max. roof drift (m)	Reduction (%)
Imperial Valley	0.0103	40.8	8.0612	12	0.0027	15.6
Kobe	0.0231	56.7	10.6058	16.8	0.0048	37.6
Kocaeli Turkey	0.0126	44	8.6356	24.6	0.0031	18
Landers	0.0121	74.8	6.4846	49	0.0027	64.9
Loma Prieta	0.0236	73	10.1686	62.8	0.0041	73
Manjil Iran	0.017	68.6	10.6662	43.5	0.0039	60.6
Southern Calif	0.017	68	9.1737	47.8	0.0039	58

Figures 9 to 11 demonstrate the displacement, acceleration, and drift diagrams in both controlled and uncontrolled modes for the five-story frame.

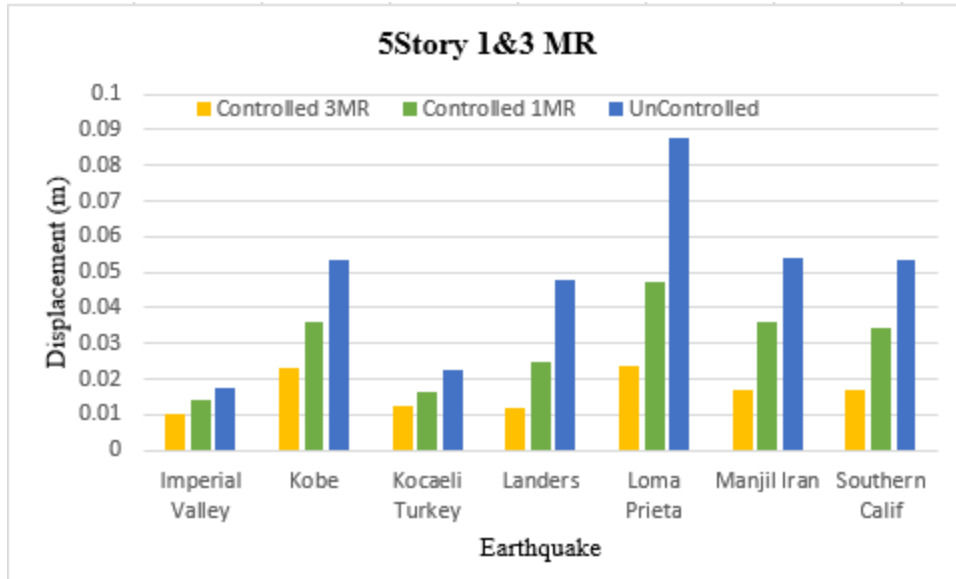


Fig. 9. Maximum roof displacement response of the five-story frame for three modes of uncontrolled, controlled with one and, three dampers.

Looking at the details in Fig. 9, the uncontrolled structure has the maximum roof displacement of 8.7cm in the Loma Prieta earthquake, and the one-damper mode structure has 4.7cm, while the three-damper mode structure has 2.3cm which is more than 50% lower than the one-damper mode structure, and almost 75% lower than the uncontrolled structure.

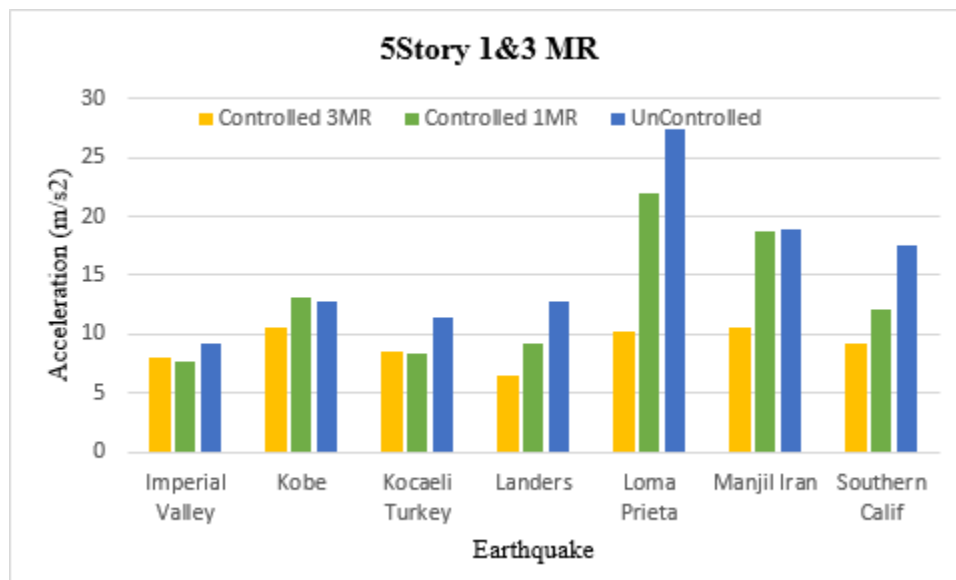


Fig. 10. Maximum roof acceleration response of the five-story frame for three modes of uncontrolled, controlled with one, and three dampers.

In Fig. 10, the uncontrolled structure had the highest acceleration response of $27.5m/s^2$ in the Loma Prieta earthquake, while the three-damper mode structure experienced only $10m/s^2$ which is almost one-third of the uncontrolled structure.

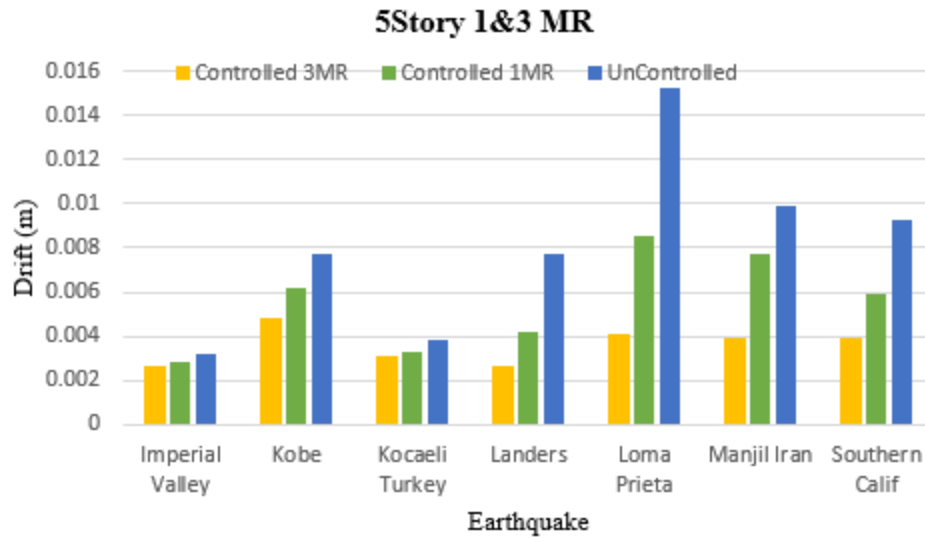


Fig. 11. Maximum drift response of the five-story frame roof for three modes of uncontrolled, controlled with one, and three dampers.

Looking at Fig. 11, the results are the same as before, leaving the three-damper mode structure as the best performer among all with a drift response of 0.4cm which is 52% lower than the one-damper structure and 73% less than the uncontrolled structure.

As can be seen from the graphs above, the three-damper mode structure has achieved better results in all of the earthquakes in terms of roof displacement, roof acceleration, and drift.

6.2. Eight-story structure

For the eight-story frame, the optimal position for the MR damper was chosen as the seventh floor. For the three-damper mode, floors one, six, and eight were selected. The results are shown in Tables 7 and 8.

Table 7

Eight-story frame responses for placing the damper on the seventh floor.

Earthquake	Max. roof displacement (m)	Reduction (%)	Max. roof acceleration (m/s^2)	Reduction (%)	Max. roof drift (m)	Reduction (%)
Imperial Valley	0.0224	28.8	8.6371	29	0.0029	32.5
Kobe	0.0985	27.7	15.5309	3	0.0101	31
Kocaeli Turkey	0.0365	32.7	11.0096	-19	0.0058	9
Landers	0.057	23.7	9.4538	16	0.0071	6.5
Loma Prieta	0.0865	38.6	10.9202	18	0.0076	38
Manjil Iran	0.0562	51.8	13.1808	17.8	0.0063	45
Southern Calif	0.0657	37	13.4366	15.9	0.0095	29.6

Table 8

Eight-story frame responses for placing the damper on floors one, six, and eight.

Earthquake	Max. roof displacement (m)	Reduction (%)	Max. roof acceleration (m/s^2)	Reduction (%)	Max. roof drift (m)	Reduction (%)
Imperial Valley	0.0161	48.8	4.7319	61	0.0026	39.5
Kobe	0.0921	32	14.6138	9	0.0099	32.6
Kocaeli Turkey	0.0309	43	8.378	8.8	0.0048	25
Landers	0.0571	23.5	10.111	10	0.0076	0
Loma Prieta	0.0415	70.5	8.9916	32.8	0.006	51
Manjil Iran	0.0407	65	8.6882	45.8	0.0059	48.7
Southern Calif	0.0502	52	10.155	36	0.0073	45.9

Figures 12 to 14 demonstrate the displacement, acceleration, and drift diagrams of the eight-story frame for three modes of uncontrolled, controlled with one and three dampers.

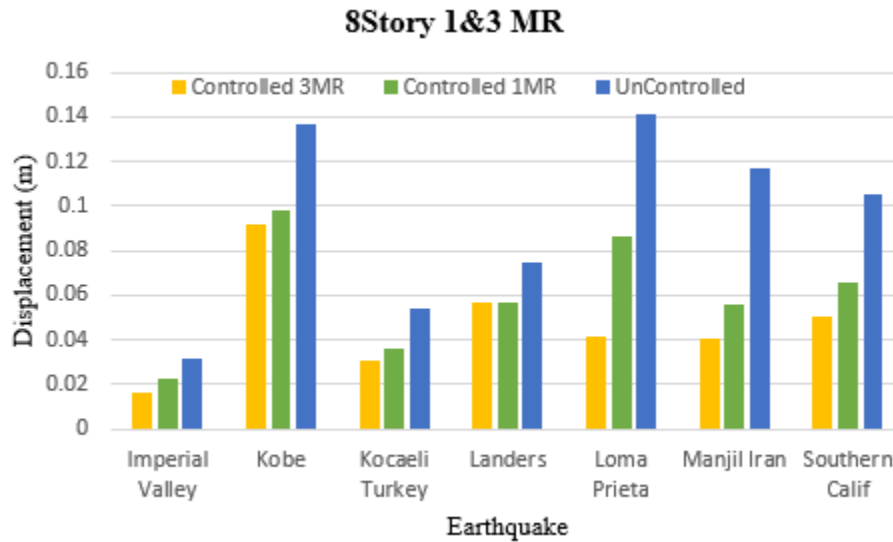


Fig. 12. Maximum roof displacement response of the eight-story frame for three modes of uncontrolled, controlled with one, and three dampers.

What stands out from Fig. 12 is that the three-damper mode structure outperforms the other two structures in all of the earthquakes.

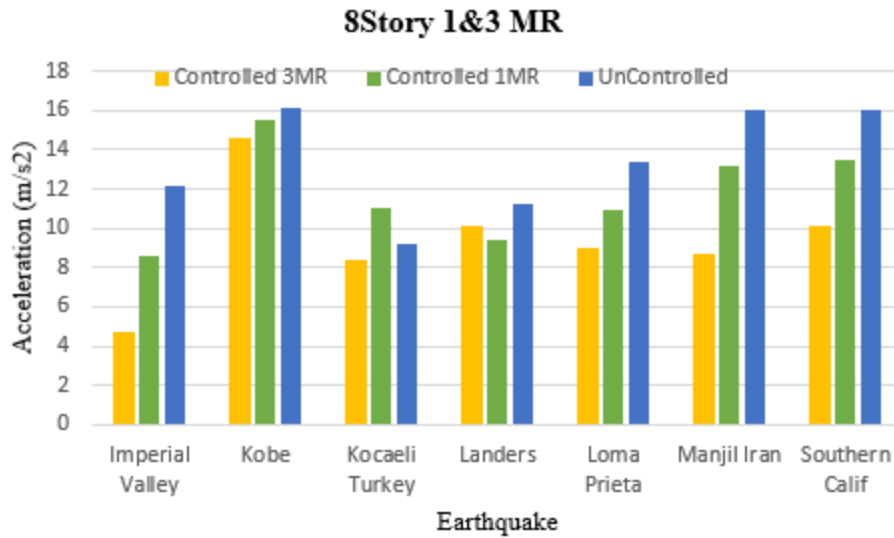


Fig. 13. Maximum roof acceleration response of the eight-story frame for three modes of uncontrolled, controlled with one, and three dampers.

Regarding Fig. 13, the three-damper mode structure had better performance in all of the earthquakes except Landers in which the one-damper mode structure had a slightly lower acceleration response.

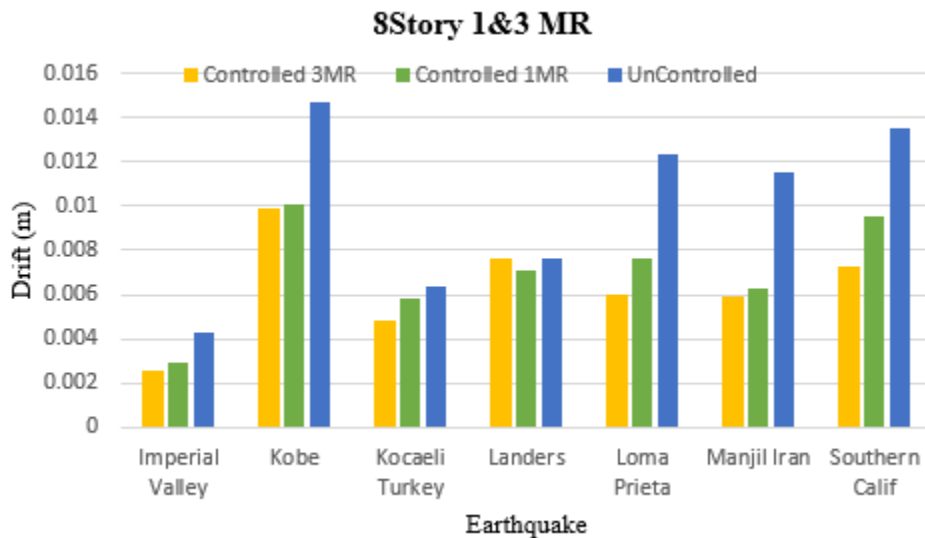


Fig. 14. Maximum drift response of the eight-story frame roof for three modes of uncontrolled, controlled with one, and three dampers.

If we look at Fig. 14, it can be seen that the three-damper mode structure had almost similar results to the one-damper mode structure in most of the earthquakes.

6.3. Eleven-story frame

For the eleven-story frame, the optimal position for the MR damper was chosen as the eleventh floor. For the three-damper mode, floors six, nine, and eleven were selected. The results are shown in Tables 9 and 10.

Table 9

Eleven-story frame responses for placing the damper on the eleventh floor.

Earthquake	Max. roof displacement (m)	Reduction (%)	Max. roof acceleration (m/s^2)	Reduction (%)	Max. roof drift (m)	Reduction (%)
Imperial Valley	0.0269	32	7.5713	5.8	0.0022	35
Kobe	0.1108	18	16.2362	-11	0.0088	23
Kocaeli Turkey	0.0878	-7	9.2574	-23	0.0067	-8
Landers	0.0848	20	9.7225	0	0.0072	20.8
Loma Prieta	0.1097	5.8	10.6579	36	0.0083	25
Manjil Iran	0.1051	4.5	12.328	-3	0.0087	0
Southern Calif	0.1168	31.8	12.8511	11	0.0096	28.8

Table 10

Eleven-story frame responses for placing the damper on floors six, nine, and eleven.

Earthquake	Max. roof displacement (m)	Reduction (%)	Max. roof acceleration (m/s^2)	Reduction (%)	Max. roof drift (m)	Reduction (%)
Imperial Valley	0.0218	45	6.0716	24.5	0.0027	20.5
Kobe	0.076	44	12.843	11.7	0.0087	24
Kocaeli Turkey	0.0336	59	7.2064	3.5	0.0043	30.6
Landers	0.075	29.5	8.8545	9	0.0059	35
Loma Prieta	0.0816	29.9	8.1498	51	0.0064	42
Manjil Iran	0.0662	39.8	11.6626	1.7	0.0057	34
Southern Calif	0.0875	48.9	12.9381	10.6	0.0077	42.9

Figures 15 to 17 demonstrate the displacement, acceleration, and drift diagrams of the eleven-story frame for three modes of uncontrolled, controlled with one and three dampers.

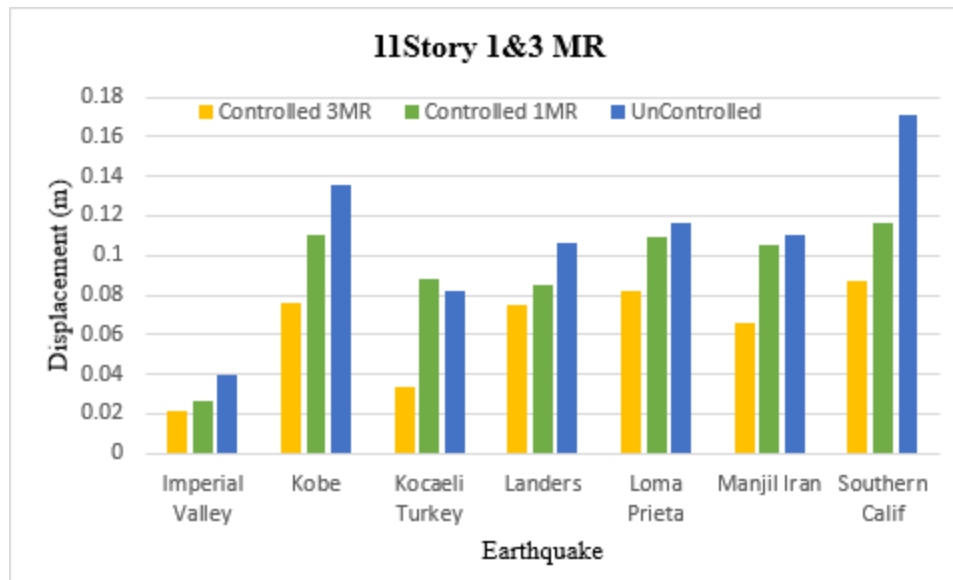


Fig. 15. Maximum roof displacement of the eleven-story frame for three modes of uncontrolled, controlled with one and three dampers.

As regards Fig. 15 it is clear that the three-damper mode structure had the best result compared to the one-damper mode, and uncontrolled structure. An interesting point is that the uncontrolled structure had less roof displacement than the one-damper mode structure in the Kocaeli earthquake.

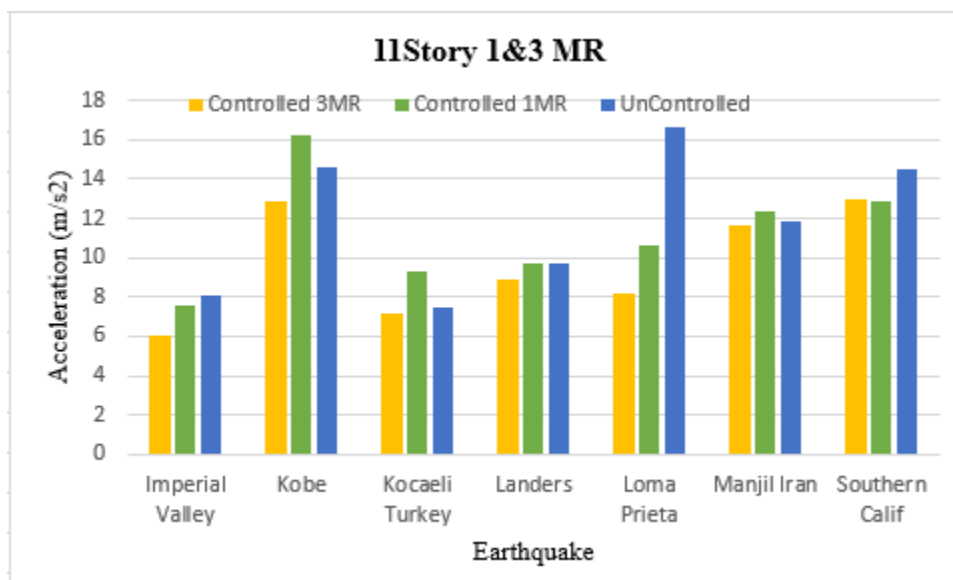


Fig. 16. Maximum roof acceleration of the eleven-story frame for three modes of uncontrolled, controlled with one and three dampers.

Looking at Fig. 16, the maximum roof acceleration belongs to the uncontrolled structure in the Loma Prieta earthquake with 16.5m/s^2 , while the three-damper mode structure experienced 8m/s^2 in the same earthquake.

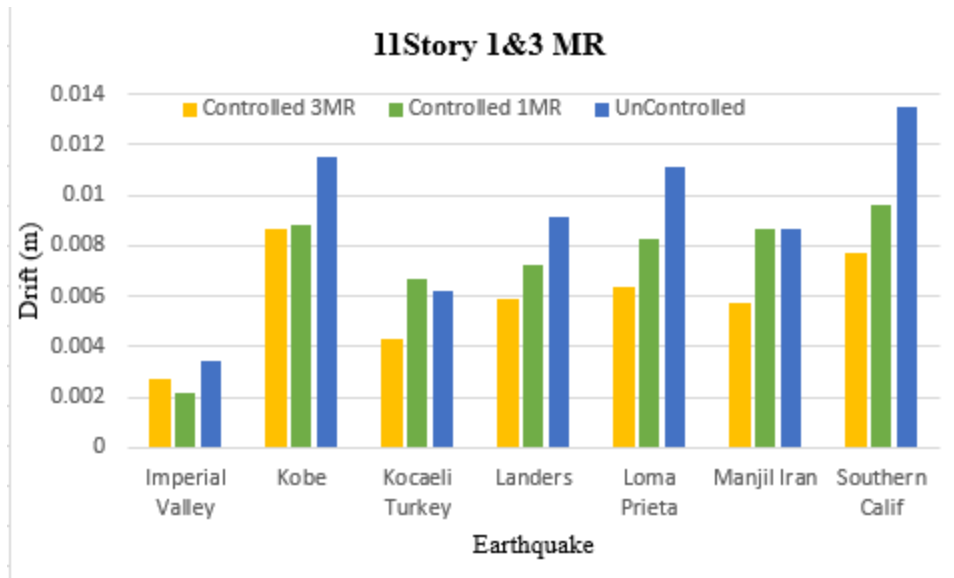


Fig. 17. Maximum drift of the eleven-story frame roof for three modes of uncontrolled, controlled with one and three dampers.

Regarding Fig. 17, the three-damper mode structure outperforms the other two structures in six out of seven earthquakes in terms of drift response. Figures 18 and 19 show the time history response of maximum displacement and acceleration for the eleven-story frame roof in both uncontrolled and controlled modes for the Imperial Valley earthquake with three dampers on floors six, nine, and eleven. It is clear that the controlled structure had much better results in terms of displacement and acceleration.

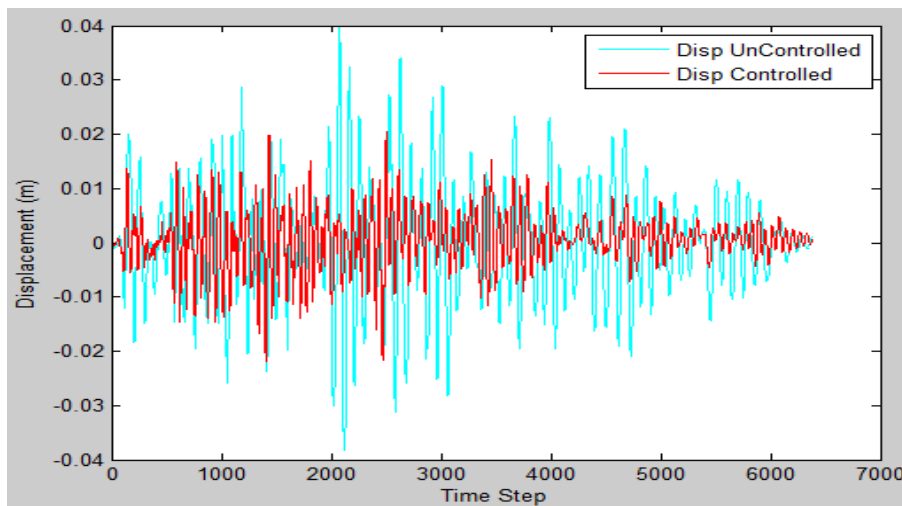


Fig. 18. Displacement time history record of the eleven-story frame in uncontrolled and controlled modes with three dampers.

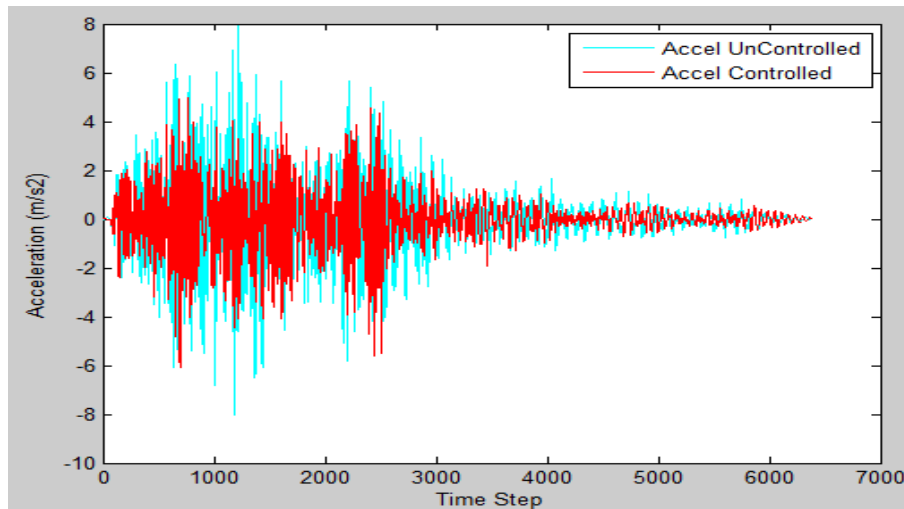


Fig. 19. Acceleration time history of the eleven-story frame in uncontrolled and controlled modes with three dampers.

7. Conclusion

1- Using optimization, a suitable control level can be achieved with a smaller number of dampers. Normally, increasing the number of MR dampers improves the reduction of structural responses, but some unfavorable situations can lead to an increase in them.

2- According to the results obtained from the five-story frame, the optimal position for the MR damper is the fifth floor. The average reduction of responses in this case for maximum displacement, acceleration, and inter-story drift of the structure is 34.6%, 17.5%, and 27.4%, respectively. For the three dampers mode, the optimal positions are the first, third and fifth floors. The average reduction of responses in this case, is equal to 60.8%, 36.6%, and 46.8%, respectively.

3- For the eight-story frame, the optimal position for the MR damper is the seventh story. The average reduction of responses in this case for maximum displacement, acceleration, and inter-story drift of the structure is 34.3%, 11.5%, and 27.3%, respectively. For the three dampers mode, the optimal positions are floors one, six, and eight. The average reduction of responses, in this case, is 47.8%, 29%, and 34.6%, respectively.

4- For the eleven-story frame, the optimal position for the MR damper is the eleventh story. The average reduction of responses in this case for maximum displacement, acceleration, and inter-story drift of the structure is 15.8%, 2.2%, and 17.8%, respectively. For the three dampers mode, the optimal positions are floors six, nine, and eleven. The average reduction of maximal displacement, acceleration, and drift responses of the structure is 42.3%, 16%, and 32.7%, respectively.

5- The best position for dampers is often the upper floors of the structure. The optimal distribution of dampers is a function of structural and earthquake characteristics. As the results show, the MR damper has a better performance in reducing displacement responses and drift compared to reducing acceleration.

References

- [1] Babaei M, Moniri A. Use of Tuned Mass Dampers in Controlling the Vibrations of Steel Structures with Vertical Irregularity of Mass. *Comput Eng Phys Model* 2018;1:83–94. <https://doi.org/10.22115/cepm.2018.137303.1035>.
- [2] Vishwakarma PN, Mishra P, Sharma SK. Characterization of a magnetorheological fluid damper a review. *Mater Today Proc* 2022;56:2988–94. <https://doi.org/10.1016/j.matpr.2021.11.143>.
- [3] Al-Fahdawi OA., Barroso LR, Soares RW. Adaptive Neuro-Fuzzy and Simple Adaptive Control Methods for Alleviating the Seismic Responses of Coupled Buildings with Semi-active Devices: Comparative Study. *Soft Comput Civ Eng* 2019;3:1–20. <https://doi.org/10.22115/SCCE.2019.199731.1128>.
- [4] Ferdaus MM, Rashid MM, Hasan MH, Rahman MA. Optimal design of Magneto-Rheological damper comparing different configurations by finite element analysis. *J Mech Sci Technol* 2014;28:3667–77. <https://doi.org/10.1007/s12206-014-0828-5>.
- [5] Nagarajaiah S, Sahasrabudhe S. Seismic response control of smart sliding isolated buildings using variable stiffness systems: an experimental and numerical study. *Earthq Eng Struct Dyn* 2006;35:177–97. <https://doi.org/10.1002/eqe.514>.
- [6] Gutierrez Soto M, Adeli H. Placement of control devices for passive, semi-active, and active vibration control of structures. *Sci Iran* 2013;20:1567–78.
- [7] Hashemi MR, Vahdani R, Gerami M, Kheyroddin A. A New Approach to the Optimal Placement of the Viscous Damper Based on the Static Force Distribution Pattern. *Period Polytech Civ Eng* 2022;66:866–75. <https://doi.org/10.3311/PPci.17238>.
- [8] Wani ZR, Tantray M. Study on integrated response-based adaptive strategies for control and placement optimization of multiple magneto-rheological dampers-controlled structure under seismic excitations. *J Vib Control* 2022;28:1712–26. <https://doi.org/10.1177/10775463211000483>.
- [9] Dyke SJ, Spencer Jr. BF, Sain MK, Carlson JD. Experimental Verification of Semi-Active Structural Control Strategies using Acceleration Feedback. *Proc. 3rd Int. Conf. Motion Vib. Control*, vol. 3, 1996, p. 291–6.
- [10] Qu WL, Xu YL. Semi-active control of seismic response of tall buildings with podium structure using ER/MR dampers. *Struct Des Tall Build* 2001;10:179–92. <https://doi.org/10.1002/tal.177>.
- [11] Zhou L, Chang C-C, Wang L-X. Adaptive Fuzzy Control for Nonlinear Building-Magnetorheological Damper System. *J Struct Eng* 2003;129:905–13. [https://doi.org/10.1061/\(asce\)0733-9445\(2003\)129:7\(905\)](https://doi.org/10.1061/(asce)0733-9445(2003)129:7(905)).
- [12] Renzi E, Serino G. Testing and modelling a semi-actively controlled steel frame structure equipped with MR dampers. *Struct Control Heal Monit* 2004;11:189–221. <https://doi.org/10.1002/stc.36>.
- [13] Yan G, Zhou LL. Integrated fuzzy logic and genetic algorithms for multi-objective control of structures using MR dampers. *J Sound Vib* 2006;296:368–82. <https://doi.org/10.1016/j.jsv.2006.03.011>.
- [14] Amini F, Ghaderi P. Optimal locations for MR dampers in civil structures using improved Ant Colony algorithm. *Optim Control Appl Methods* 2012;33:232–48. <https://doi.org/10.1002/oca.991>.
- [15] Askari M, Li J, Samali B. Cost-effective multi-objective optimal positioning of magnetorheological dampers and active actuators in large nonlinear structures. *J Intell Mater Syst Struct* 2017;28:230–53. <https://doi.org/10.1177/1045389X16649449>.
- [16] Lopes MA, Soeiro FJCP, Santos da Silva JG. Structural optimization of concrete volume for machine foundation using genetic algorithms. *J Soft Comput Civ Eng* 2019;3:62–81. <https://doi.org/10.22115/SCCE.2019.203066.1129>.
- [17] Sanaei E, Babaei M. Cellular Automata in Topology Optimization of Continuum Structures. *Int J Eng Sci Technol* 2011;3. <https://doi.org/10.4314/ijest.v3i4.68539>.

- [18] Hasańcebi O, arbař S, Dođan E, Erdal F, Saka MP. Performance evaluation of metaheuristic search techniques in the optimum design of real size pin jointed structures. *Comput Struct* 2009;87:284–302. <https://doi.org/10.1016/j.compstruc.2009.01.002>.
- [19] Rajeev S, Krishnamoorthy CS. Discrete optimization of structures using genetic algorithms. *J Struct Eng* 1992;118:1233–50.
- [20] Akbari M, Henteh M. Comparison of Genetic Algorithm (GA) and Particle Swarm Optimization Algorithm (PSO) for Discrete and Continuous Size Optimization of 2D Truss Structures. *J Soft Comput Civ Eng* 2019;3:76–97. <https://doi.org/10.22115/SCCE.2019.195713.1117>.
- [21] Fathali MA, Hoseini Vaez SR. Optimum performance-based design of eccentrically braced frames. *Eng Struct* 2020;202:109857. <https://doi.org/10.1016/j.engstruct.2019.109857>.
- [22] Abedini H, Hoseini Vaez SR, Zarrineghbal A. Optimum design of buckling-restrained braced frames. *Structures* 2020;25:99–112. <https://doi.org/10.1016/j.istruc.2020.03.004>.
- [23] Babaei M, Mollayi M. An improved constrained differential evolution for optimal design of steel frames with discrete variables. *Mech Based Des Struct Mach* 2020;48:697–723. <https://doi.org/10.1080/15397734.2019.1657890>.
- [24] Seraji N, Babaei M. Discrete sizing optimization of steel structures using modified fireworks algorithm n.d.
- [25] Sanaei E, Babaei M. Topology optimization of structures using cellular automata with constant strain triangles. *Int J Civ Eng* 2012;10:179–88.
- [26] Camp C V., Bichon BJ, Stovall SP. Design of Steel Frames Using Ant Colony Optimization. *J Struct Eng* 2005;131:369–79. [https://doi.org/10.1061/\(ASCE\)0733-9445\(2005\)131:3\(369\)](https://doi.org/10.1061/(ASCE)0733-9445(2005)131:3(369)).
- [27] Kaveh A, Talatahari S. An improved ant colony optimization for the design of planar steel frames. *Eng Struct* 2010;32:864–73. <https://doi.org/10.1016/j.engstruct.2009.12.012>.
- [28] Talatahari S, Nouri M, Tadbiri F, Branch S, Azad I. OPTIMIZATION OF SKELETAL STRUCTURAL USING. *Int J Optim Civ Eng* 2012;2:557–71.
- [29] Farshchin M, Maniat M, Camp C V., Pezeshk S. School based optimization algorithm for design of steel frames. *Eng Struct* 2018;171:326–35. <https://doi.org/10.1016/j.engstruct.2018.05.085>.
- [30] Pezeshk S, Camp C V., Chen D. Design of Nonlinear Framed Structures Using Genetic Optimization. *J Struct Eng* 2000;126:382–8. [https://doi.org/10.1061/\(ASCE\)0733-9445\(2000\)126:3\(382\)](https://doi.org/10.1061/(ASCE)0733-9445(2000)126:3(382)).
- [31] Babaei M. Multi-objective optimal number and location for steel outrigger-belt truss system. *J Eng Sci Technol* 2017;12:2599–612.
- [32] Babaei M, Sanaei E. Multi-objective optimal design of braced frames using hybrid genetic and ant colony optimization. *Front Struct Civ Eng* 2016;10:472–80. <https://doi.org/10.1007/s11709-016-0368-4>.
- [33] Babaei M, Mollayi M. Multi-objective Optimization of Reinforced Concrete Frames Using NSGA-II Algorithm. *Eng Struct Technol* 2016;8:157–64. <https://doi.org/10.3846/2029882X.2016.1250230>.
- [34] Ghasemof A, Mirtaheri M, Karami Mohammadi R. Effects of demand parameters in the performance-based multi-objective optimum design of steel moment frame buildings. *Soil Dyn Earthq Eng* 2022;153:107075. <https://doi.org/10.1016/j.soildyn.2021.107075>.
- [35] Ghasemof A, Mirtaheri M, Karami Mohammadi R. Multi-objective optimization for probabilistic performance-based design of buildings using FEMA P-58 methodology. *Eng Struct* 2022;254:113856. <https://doi.org/10.1016/j.engstruct.2022.113856>.
- [36] Jung H-J, Spencer BF, Lee I-W. Control of Seismically Excited Cable-Stayed Bridge Employing Magnetorheological Fluid Dampers. *J Struct Eng* 2003;129:873–83. [https://doi.org/10.1061/\(ASCE\)0733-9445\(2003\)129:7\(873\)](https://doi.org/10.1061/(ASCE)0733-9445(2003)129:7(873)).
- [37] Ok S-Y, Kim D-S, Park K-S, Koh H-M. Semi-active fuzzy control of cable-stayed bridges using magneto-rheological dampers. *Eng Struct* 2007;29:776–88. <https://doi.org/10.1016/j.engstruct.2006.06.020>.